The dual nature of bacteriophage: growth-dependent predation and generalised transduction of antimicrobial resistance

Quentin J Leclerc[1,2]*, Jacob Wildfire[2,3], Arya Gupta[3+], Jodi A Lindsay[3], Gwenan M Knight[1,2]

[1] Centre for Mathematical Modelling of Infectious Diseases, Department of Infectious Disease Epidemiology, Faculty of Epidemiology & Population Health, London School of Hygiene & Tropical Medicine, UK

[2] Antimicrobial Resistance Centre, London School of Hygiene and Tropical Medicine, UK

[3] Institute for Infection & Immunity, St George's University of London, UK

[+] Present address: School of Biosciences, University of Kent, UK

* corresponding author: quentin.leclerc@lshtm.ac.uk

Abstract

Bacteriophage ("phage") are both predators and evolutionary drivers for bacteria, notably contributing to the spread of antimicrobial resistance (AMR) genes by generalised transduction. Our current understanding of the dual nature of this relationship is limited. We used an interdisciplinary approach to quantify how these interacting dynamics can lead to the evolution of multi-drug resistant bacteria. We co-cultured two strains of Methicillin-resistant *Staphylococcus aureus*, each harbouring a different antibiotic resistance gene, with 80α generalized transducing phage. After a growth phase of 8h, bacteria and phage surprisingly coexisted at a stable equilibrium in our culture, the level of which was dependent on the starting concentration of phage. We detected double-resistant bacteria as early as 7h, indicating that transduction of AMR genes had occurred. We developed multiple mathematical models of the bacteria and phage relationship, and found that phage-bacteria dynamics were best captured by a model in which the phage burst size decreases as the bacteria population reaches stationary phase, and where phage predation is frequency-dependent. We estimated that one in every 10^8 new phage generated was a transducing phage carrying an AMR gene, and that double-resistant bacteria were always predominantly generated by transduction rather than by growth. Our results suggest a shift in how we understand and model phage-bacteria dynamics. Although rates of generalised transduction could be interpreted as too rare to be significant, they are sufficient to consistently lead to the evolution of multi-drug resistant bacteria. Currently, the potential of phage to contribute to the growing burden of AMR is likely underestimated.

Introduction

To counter the rapidly increasing global public health threat of antimicrobial resistance (AMR), we must urgently develop new solutions [1]. "Phage therapy" is one such tool which has recently seen a renewed interest [2]. This relies on using bacteriophage (or "phage"), major bacteria predators and the most abundant biological entities on the planet [3], as antimicrobial agents. However, phage are also natural drivers of bacterial evolution through horizontal gene transfer by "transduction" [4,5]. AMR genes can be transferred by transduction at high rates, both *in vitro* and *in vivo* [6–8]. The dual nature of phage (predation and transduction) makes them a double-edged sword in the fight against AMR, as they are themselves capable of contributing to the spread of the problem they aim to solve, yet our understanding of these dynamics and how to best represent them is limited.

There are two types of transduction; here, we focus on "generalised transduction", which occurs during the phage lytic cycle, when non-phage genome DNA is mistakenly packaged in a new phage particle (Figure 1). The resulting transducing phage released upon lysis can then inject this genetic material into another bacterium. Current guidelines for phage therapy recommend that exclusively lytic phage should be used, removing the risk of the second type of transduction which relies on lysogeny ("specialised transduction", where sections of bacterial DNA adjacent to the prophage integration site may be transferred upon excision of the prophage) [9,10]. The possibility of generalised transduction remains, yet is currently often dismissed as too rare to be significant, despite being a common mechanism for the transfer of plasmids, major vectors of AMR genes [4]. Alternatively, guidelines may state that the risk of generalised transduction should be minimised [9,11,12], yet there are currently no estimates or work quantifying what constitutes an "acceptable" risk. Previous reviews have highlighted the necessity to further investigate the potential impact of transduction in the context of phage therapy [11–13].

56 Mathematical models have been used to gain insights into phage predation dynamics which cannot
57 be obtained solely with experimental work, such as rates of predation and optimal conditions for
58 phage to clear bacteria [14]. Such models typically assume a density-dependent interaction, with new
59 phage infections calculated as the number of susceptible bacteria, multiplied by the number of phage
60 and an adsorption constant [14–16]. This approach has limitations, as density-dependent models have
61 failed to predict equilibriums observed in some *in vitro* conditions between phage and *E. coli* [17].
62 Moreover, phage and bacterial replication are likely to be linked, as they both rely on the bacterial
63 machinery; phage predation may slow as bacteria reach stationary phase [14,17–23]. However, this is a
64 feature which is not commonly included in mathematical models of phage-bacteria dynamics [14].
65 Finally, models often only rely on data of phage-bacteria interactions measured once per day, or for a
66 few hours [17–19,24]. A current lack of detailed data means that capturing these underlying dynamics
67 which occur in less than an hour has not yet been possible.

68 To the best of our knowledge, only three modelling studies have included transduction of AMR genes
69 [25–27]. All three modelled complex environments, including resistance to phage, antibiotics, and both
70 lytic and lysogenic cycles. This complexity, combined with the fact that these studies were not paired
71 with complementary *in vitro* or *in vivo* data, means that they relied on assumptions and previously
72 published estimates, instead of parameter values derived from a single environment and set of
73 conditions. This limits the wider reliability of conclusions made using these models [13].

74 In this article, we investigate the dual nature of phage dynamics using the clinically relevant bacteria
75 Methicillin-resistant *Staphylococcus aureus* (MRSA) [28]. Transduction is the main mechanism of
76 horizontal gene transfer driving evolution for these bacteria [29], and phage therapy is currently being
77 investigated to treat MRSA infections [30,31]. We aim to clarify the dual nature (predation and
78 transduction) of the interaction between MRSA and phage by generating novel *in vitro* data,
79 identifying biologically plausible hypotheses which may explain the dynamics seen, and developing
80 mathematical models to test the validity of these hypotheses in our system.

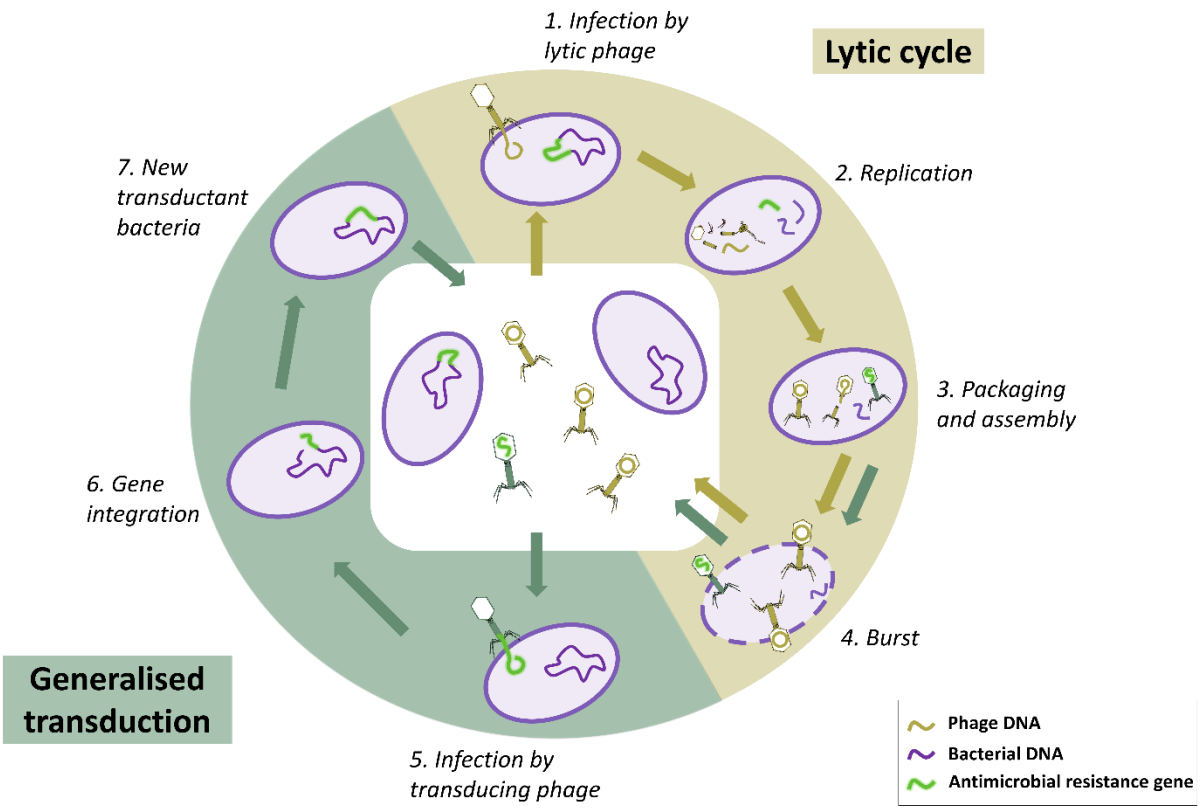

Figure 1: Phage lytic cycle and generalised transduction. In this environment, only some bacteria carry an antimicrobial resistance (AMR) gene (shown in green). The lytic cycle starts when a lytic phage infects a bacterium by binding and injecting its DNA (1). Phage molecules degrade bacterial DNA and utilise bacterial resources to create new phage components and replicate (2). These components are then assembled to form new phage particles (3). At this stage, bacterial DNA leftover in the cell can be packaged by mistake instead of phage DNA, which creates a transducing phage and starts the process of generalised transduction. In our example, the transducing phage carries the AMR gene. After a latent period of typically several minutes, the phage trigger lysis of the bacterium, bursting it and releasing the phage (4). The transducing phage can infect another bacterium, binding and injecting the AMR gene it is carrying (5). If this gene is successfully integrated into the bacterial chromosome (6), this creates a new transductant bacterium carrying this AMR gene (7). Note that the transduced bacterial DNA could also be a plasmid, in which case it would circularise instead of integrating into the chromosome of the transductant bacterium. Not to scale.

95 # Results

96 ## Transduction and phage predation dynamics *in vitro*

97 We focused on two laboratory strains of *Staphylococcus aureus*, each resistant to either erythromycin
98 (and referred to as B_E) or tetracycline (B_T). In our experimental conditions, the antimicrobial resistance
99 (AMR) genes can only be transferred between bacteria by generalised transduction mediated by
100 exogenous phage. Transduction of either AMR gene to the other strain will result in the formation of
101 double-resistant progeny (referred to as B_{ET}).

102 We conducted a co-culture with only the two single-resistant strains and exogenous temperate phage
103 80α (P_L) capable of generalised transduction. We grew the bacteria and phage over 24h, with hourly
104 counts of bacteria and lytic phage between 0-8h and 16-24h. The starting concentration of bacteria
105 was 10^4 colony-forming units (cfu) per mL, and of phage was approximately either 10^3, 10^4 or 10^5
106 plaque-forming units (pfu) per mL, equivalent to multiplicities of infection of 0.1, 1 and 10 (defined as
107 starting ratio of phage to bacteria [32]).

108 We detected double-resistant progeny (B_{ET}) as early as 7h in our co-cultures, indicating that transfer
109 of AMR genes by generalised transduction had occurred (Figure 2). B_{ET} numbers remained below 100
110 cfu/mL after 24h, but were consistently generated in each of our experimental replicates. Colonies of
111 double-resistant progeny were screened using polymerase chain reaction (PCR) to confirm that they
112 contained both resistance genes *ermB* and *tetK*, and had not instead gained resistance to either
113 antibiotic by mutation (Figure 2 – figure supplement 1).

114 The starting concentration of exogenous phage affected whether phage and bacteria were able to
115 reach an equilibrium and co-exist without increasing or decreasing in our co-cultures (Figure 2). With
116 a starting concentration of either 10^3 or 10^4 pfu/mL, lytic phage reached a steady-state after 8h (at
117 approximately 10^5 pfu/mL for a starting concentration of 10^3, and 10^7 pfu/mL for 10^4). In both cases,

118 bacteria replicated for 8h before reaching a steady-state around 10^9 cfu/mL, similar to what was seen
119 in the absence of exogenous phage (Figure 2 – figure supplement 2). With a starting phage
120 concentration of 10^5 pfu/mL, we did not see an equilibrium between phage and bacteria, as phage
121 numbers kept increasing up to 10^{10} pfu/mL by 24h, and bacteria numbers started decreasing after
122 20h. The datasets are shown overlaid in Figure 2 – figure supplement 3.

123

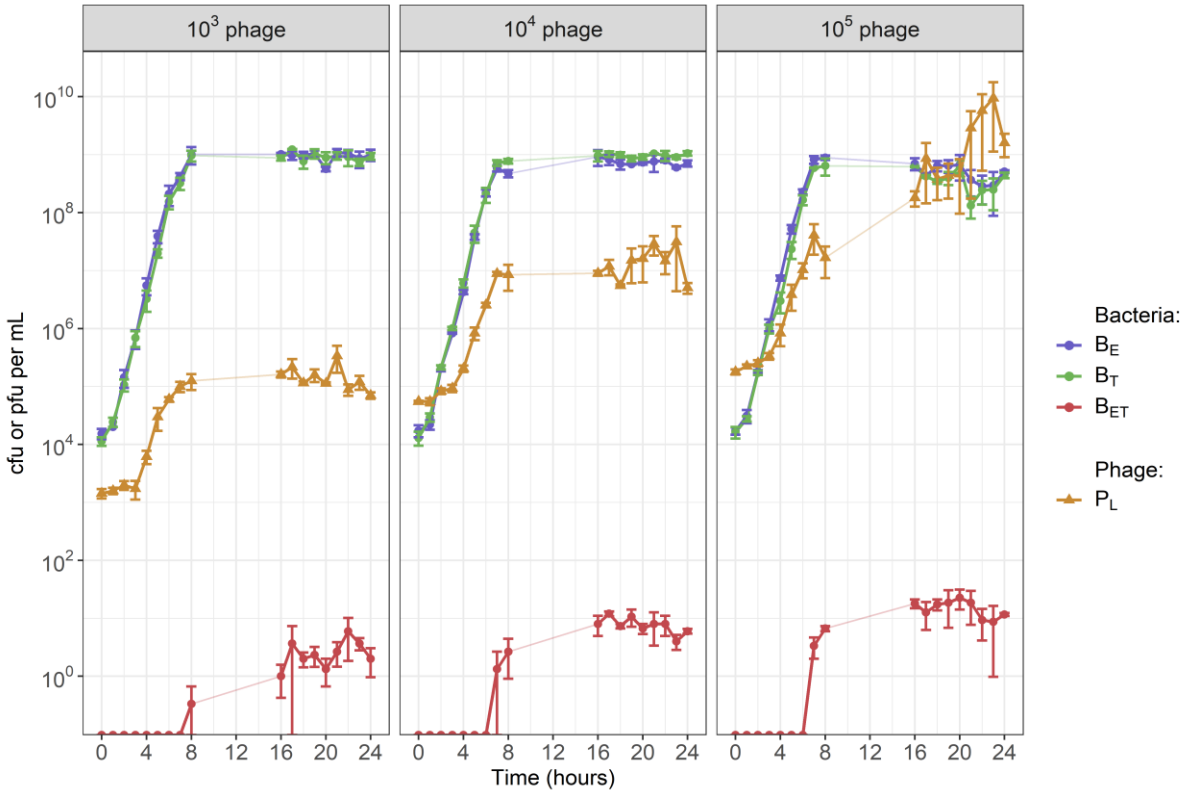

124

125 **Figure 2: The starting concentration of exogenous phage 80α affected the equilibrium values of**
126 **phage and bacteria in our co-cultures.** The starting concentration of both single-resistant *S. aureus*
127 parent strains (B_E to erythromycin & B_T to tetracycline) was 10^4 colony-forming units (cfu) per mL. Each
128 panel shows the results with a different starting concentration of exogenous phage 80α (P_L): either
129 10^3, 10^4 or 10^5 plaque-forming units (pfu) per mL. We detected double-resistant progeny (B_{ET}) as early
130 as 7h, indicating that transduction occurred rapidly. Error bars indicate mean +/- standard error, from
131 3 experimental replicates. There is no data for the time period 9h-15h. **Figure supplement 1:**

132 **Confirmation of double-resistant progeny by polymerase-chain reaction.** Five single colonies were
133 sampled from a double antibiotic plate (1-5), containing bacteria plated after 24h of co-culture started
134 only with single-resistant parent strains (E and T) and exogenous phage. L: ladder; E: erythromycin
135 resistance gene (*ermB*); T: tetracycline resistance gene (*tetK*). **Figure supplement 2: Growth curves**
136 **for bacteria in the absence of exogenous phage.** Solid lines correspond to *in vitro* data, and dashed
137 lines to the model output generated using the median values of the parameter distributions obtained
138 by model fitting. Shaded areas indicate error obtained by resampling the model results from a Poisson
139 distribution ten times. **Figure supplement 3: Transduction co-culture datasets overlaid.**

140

141 Absence of lysogeny in our co-culture

142 80α is a temperate phage, which means that it may undergo lysogeny and integrate in the bacterial
143 chromosome as a prophage [33]. This would grant lysogenic immunity to the bacteria, preventing further
144 lytic infection by 80α, and potentially explaining why bacteria and phage densities reached steady-
145 states in our experiments (Figure 2). To investigate this, we initiated co-cultures with 10^4 cfu/mL of
146 each single-resistant strain and 10^4 pfu/mL of 80α phage. After 24h, we diluted these in fresh media
147 to form new co-cultures with an inocula of 10^4 cfu/mL of bacteria already exposed to the phage, and
148 added phage to reach a concentration of 10^4 pfu/mL again. We did not see any difference in phage
149 and bacteria numbers after 24h regardless of whether or not the bacteria had been previously
150 exposed to phage (Figure 3a).

151 In addition, we extracted DNA from the co-cultures after 24h, and conducted PCRs targeting the
152 prophage junctions (*attL* and *attR*) and bacterial insertion site (*attB*). Only the intact bacterial insertion
153 site was detected in our samples, indicating an absence of prophage in our bacteria (Figure 3b).
154 Overall, these results suggest that lysogeny does not occur at a detectable level in our co-culture, and
155 that we can exclude any dynamics relating to lysogeny in our analysis and model below.

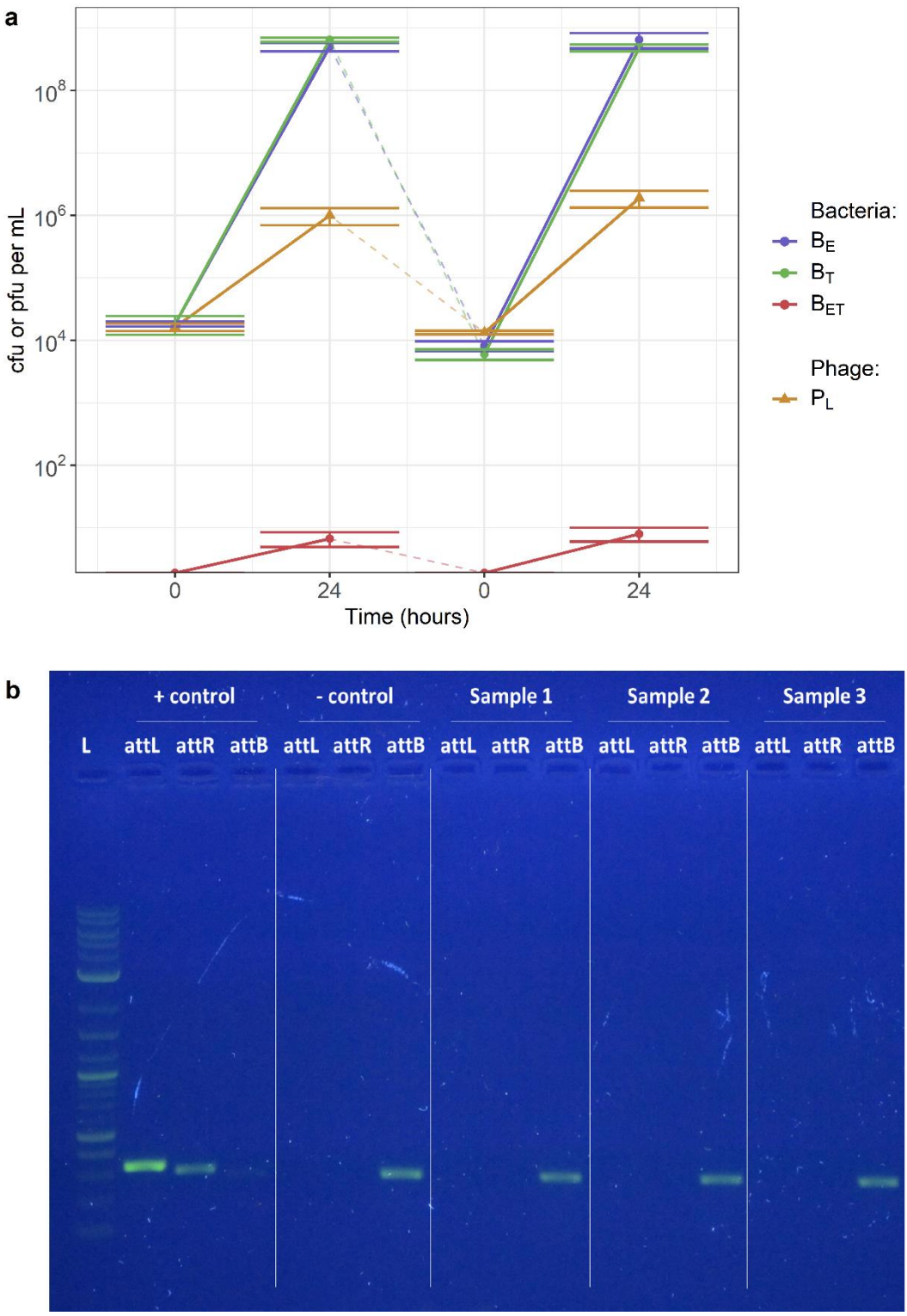

156

157 **Figure 3: 80α lysogeny does not occur at a detectable level in our co-culture. (a) Co-cultures with**

158 **bacteria not exposed or previously exposed to phage.** The starting concentration of both single-

159 resistant *S. aureus* parent strains (B_E to erythromycin & B_T to tetracycline) was 10^4 colony-forming

160 units (cfu) per mL, and the starting concentration of exogenous phage 80α (P_L) was 10^4 plaque-forming

161 units (pfu) per mL. Double-resistant progeny (B_{ET}) are generated by transduction. The initial co-culture
162 was diluted in fresh media after 24h, to form a new co-culture with bacteria previously exposed to
163 phage. Phage were added in the new co-culture to reach a concentration of 10^4 pfu/mL. Error bars
164 indicate mean +/- standard error, from 3 experimental replicates. **(b) Confirmation of absence of**
165 **detectable lysogeny by polymerase-chain reaction.** DNA was extracted from the co-cultures after
166 24h. *S. aureus* RN4220 strains lysogenic and non-lysogenic for 80α were used as positive and negative
167 controls. L: ladder; *attL*: left prophage junction; *attR*: right prophage junction; *attB*: bacterial insertion
168 site. Detection of *attL* and *attR* indicates that prophage are present in the DNA, while detection of
169 *attB* indicates the presence of bacteria not lysogenic for 80α.

170

171 Bacterial growth estimates in the absence of exogenous phage

172 When grown together in the absence of exogenous phage, single and double resistant bacteria
173 replicated exponentially and reached stationary phase after 8h at 10^9 colony-forming units (cfu) per
174 mL (Figure 2 – figure supplement 2). For each pair of strains, we estimated relative fitness *W* using
175 Equation 1.

176 $$W = \frac{ln[\frac{S1(24)}{S1(0)}]}{ln[\frac{S2(24)}{S2(0)}]} \qquad (1)$$

177 Where S1(*t*) and S2(*t*) represent the number of bacteria (in cfu/mL) from the chosen strains 1 and 2,
178 at times *t* = 0 or 24 hours.

179 B_E did not show a significant fitness cost relative to B_T over 24h of growth (mean relative fitness 1.02,
180 sd 0.03). The double-resistant progeny B_{ET} did not show a significant fitness cost relative to either
181 single-resistant parent strain (mean relative fitness to B_E: 0.96, sd 0.06; mean relative fitness to B_T:
182 0.98, sd 0.03).

183 We obtained maximum growth rate estimates by fitting a logistic growth model to the *in vitro* data.
184 This is shown in Equation 2, where μ_{max} is the maximum bacterial growth rate, B_{max} is the carrying
185 capacity, and *B* the concentration of bacteria (in cfu/mL).

186 $$\frac{dB}{dt} = \mu_{max} * B * \left(1 - \frac{B}{B_{max}}\right) \quad (2)$$

187 The median estimated maximum growth rates were 1.61 for B_E (95% credible interval 1.59-1.63), 1.51
188 for B_T (1.49-1.53) and 1.44 for B_{ET} (1.42-1.47), with a total carrying capacity of 2.76 x 10^9 cfu/mL (2.61
189 x 10^9 - 2.98 x 10^9).

190 Investigation of possible phage-bacteria interactions using a flexible
191 modelling framework

192 *Model structure*

193 We designed a mathematical model to reproduce the *in vitro* phage-bacteria dynamics, including
194 generalised transduction of resistance genes. During our experiment, our co-culture contained up to
195 three strains of bacteria: the two single-resistant parents (B_E, B_T) and the double-resistant progeny
196 (B_{ET}). Although we were only able to count lytic phage (P_L), based on the biology of generalised
197 transduction (Figure 1) we know that there were also transducing phage carrying either the
198 erythromycin resistance gene (P_E), or the tetracycline resistance gene (P_T). Since we did not detect any
199 evidence of 80α lysogeny in our co-culture after 24h, we did not include this feature in the model. The
200 corresponding model diagram is shown in Figure 4a. The complete model equations can be found in
201 Methods.

202 Using this modelling framework, we explored a combination of different phage-bacteria interactions,
203 described below (Figure 4b-c). By fitting the models to our experimental data, we could rule out
204 certain interactions and suggest the best model to reproduce the phage-bacteria dynamics seen *in*
205 *vitro*.

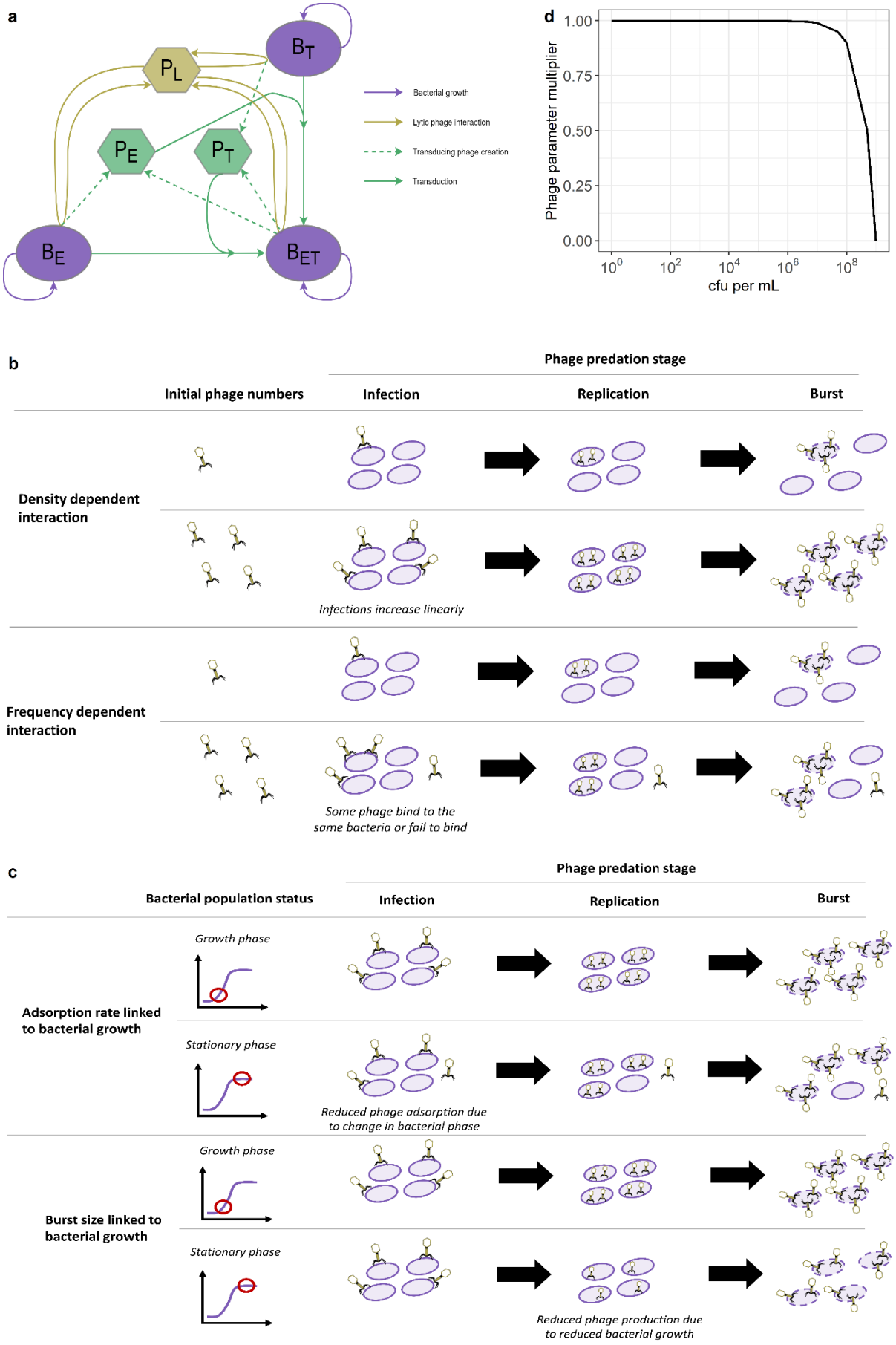
a
B_T
P_L
P_E
P_T
B_E
B_{ET}
Bacterial growth
Lytic phage interaction
Transducing phage creation
Transduction
d
Phage parameter multiplier
1.00
0.75
0.50
0.25
0.00
10^0
10^2
10^4
10^6
10^8
cfu per mL
b
Phage predation stage
Initial phage numbers
Infection
Replication
Burst
Density dependent interaction
Infections increase linearly
Frequency dependent interaction
Some phage bind to the same bacteria or fail to bind
c
Phage predation stage
Bacterial population status
Infection
Replication
Burst
Adsorption rate linked to bacterial growth
Growth phase
Stationary phase
Reduced phage adsorption due to change in bacterial phase
Burst size linked to bacterial growth
Growth phase
Stationary phase
Reduced phage production due to reduced bacterial growth

206

207 **Figure 4: Phage predation and generalised transduction model diagram, and different phage-**
208 **bacteria interactions considered.** (**a) Model diagram.** Each bacteria strain (B_E resistant to
209 erythromycin, B_T resistant to tetracycline, or B_{ET} resistant to both) can replicate (purple). The lytic
210 phage (P_L) multiply by infecting a bacterium and bursting it to release new phage (gold). This process
211 can create transducing phage (P_E or P_T) carrying a resistance gene (*ermB* or *tetK* respectively) taken
212 from the infected bacterium (green). These transducing phage can then generate new double resistant
213 progeny (B_{ET}) by infecting the bacteria strain carrying the other resistance gene (green). **(b) Phage**
214 **predation in the model is either density- or frequency-dependent.** With a density-dependent
215 interaction, the number of infections scales linearly with the number of phage and bacteria (top). A
216 frequency-dependent interaction illustrates that some phage may not infect a bacterium, or that
217 multiple phage may infect the same bacterium (bottom). **(c) Phage predation in the model can**
218 **decrease as bacterial growth decreases.** A change in bacterial growth phase can affect surface
219 receptors, leading to a reduced phage adsorption rate (top). Since phage replication relies on bacterial
220 processes, a reduced bacterial growth can translate into a reduced phage burst size (bottom). **(d)**
221 **Proposed function linking phage predation parameters to bacterial growth.** This shows the multiplier
222 applied to decrease phage parameters as the bacterial population increases towards carrying capacity,
223 equivalent to a decrease in bacterial growth. Here, the carrying capacity is 2.76 x 10^9 colony-forming
224 units (cfu)/mL, estimated from our data.

225

226 *First phage-bacteria interaction: density versus frequency-dependent phage predation*

227 The most common approach to model phage-bacteria dynamics is to assume that phage predation is
228 density-dependent [14]. This means that, over one time step, the number of phage infecting bacteria
229 and the number of bacteria infected by phage are both equal to the product of the number of bacteria
230 (B), phage (P), and phage adsorption rate (β), as shown in equation (3).

231 $$B * P * \beta \qquad (3)$$

232 The density-dependent interaction implies that the number of new infections scales linearly with the
233 number of phage and bacteria (Figure 4b). Therefore, even if we keep a constant number of phage,
234 increasing bacteria numbers always leads to a linear increase in the estimated number of new
235 infections. Although this simplification is useful and holds for a range of values, it has been suggested
236 that it is not biologically realistic for small numbers of phage or bacteria, since in reality one phage can
237 only infect one bacterium over one time step [17].

238 To overcome these issues, we consider an alternative interaction, where phage predation is
239 frequency-dependent [34]. This accounts for the fact that one phage does not necessarily always lead to
240 one infection. For example, phage may sometimes fail to bind to bacteria, or multiple phage may bind
241 to the same bacterium [32] (Figure 4b). Importantly, this mathematical interaction guarantees that, at
242 any given time point, the number of phage infecting bacteria and the number of bacteria infected by
243 phage can never be greater than the total number of phage or bacteria in the system. Over one time
244 step, the proportion of phage infecting any bacteria (λ) is defined by equation (4).

245 $$\lambda = (1 - exp\ (-\beta * B)\ ) \qquad (4)$$

246 Similarly, the proportion of bacteria being infected by at least one phage (φ) is calculated with
247 equation (5).

248 $$\varphi = \left(1 - exp\ \left(-\frac{\lambda * P}{B}\right)\right) \qquad (5)$$

249

250 *Equilibrium analyses for the density and frequency-dependent models*

251 Despite these being common methods to represent phage-bacteria interactions in mathematical
252 models, previous analyses have suggested that the density and frequency-dependent interactions
253 alone cannot capture the equilibrium levels we and others have seen [18,35]. We explore this in the
254 context of our own *in vitro* data using equilibrium analyses.

255 Assuming that transduction and the phage latent period are negligible, a simplified model
256 representing phage predation as a density-dependent process is shown in equations (6) and (7).

257 $$\frac{dB}{dt} = \mu_{max} * B * (1 - \frac{B}{B_{max}}) - B * P * \beta \qquad (6)$$

258 $$\frac{dP}{dt} = B * P * \beta * \delta' - \gamma * P \qquad (7)$$

259 Where μ_{max} is the maximum bacterial growth rate, B_{max} is the carrying capacity, β is the phage
260 adsorption rate, γ is the phage decay rate, and δ is the phage burst size, with δ' equal to δ - 1. To solve
261 for equilibrium (i.e. $\frac{dB}{dt} = \frac{dP}{dt} = 0$), equations (6) and (7) can be rewritten as equations (8) and (9).

262 $$\mu_{max} * B * (1 - \frac{B}{B_{max}}) - B * P * \beta = 0 \qquad (8)$$

263 $$B * P * \beta * \delta' - \gamma * P = 0 \qquad (9)$$

264 Since we are interested in an equilibrium with the condition that there are still bacteria and phage in
265 the environment (i.e. B≠0 and P≠0), we can divide equations (8) and (9) by B and P respectively to
266 obtain equations (10) and (11). These must hold true for there to be a non-zero bacteria and phage
267 population at equilibrium.

268 $$\mu_{max} * (1 - \frac{B}{B_{max}}) - P * \beta = 0 \qquad (10)$$

269 $$B * \beta * \delta' - \gamma = 0 \qquad (11)$$

270 We then obtain equations (12) and (13) by rearranging (10) and (11) to give expressions for P and B at
271 equilibrium.

272 $$P = \frac{\mu_{max}}{\beta} * (1 - \frac{B}{B_{max}}) \ (12)$$

273 $$B = \frac{\gamma}{\beta * \delta'} \qquad (13)$$

274 In our experiment with a starting phage concentration of 10^4 plaque-forming units (pfu)/mL, after 24h
275 the bacteria concentration was approximately 10^9 colony-forming units (cfu)/mL, and the phage

concentration was 10^5 pfu/mL. If we replace the corresponding terms in equations (12) and (13) with these values, alongside the carrying capacity (2.8 x 10^9) and average of the growth rates estimated (1.52), we obtain equations (14) and (15).

$$10^5 = \frac{1.52}{\beta} * (1 - \frac{10^9}{2.8*10^9}) \qquad (14)$$

$$10^9 = \frac{\gamma}{\beta * \delta'} \qquad (15)$$

Rearrangement of equation (14) leads to a solution for phage adsorption (β) (equation (16)).

$$\beta = 9.77 * 10^{-6} \approx 10^{-5} \qquad (16)$$

Substituting this into equation (15) leads to a value for phage decay rate (γ) (equation (17)).

$$\gamma = 10^9 * 10^{-5} * \delta' \approx 10^4 * \delta' \qquad (17)$$

Giving rise to the condition that the phage decay rate γ must be approximately 10^4 times greater than the burst size δ'. As at least one phage must be released upon bursting, the burst size δ' is greater than 1. However, the phage decay rate γ, which represents the proportion of phage inactivated during one time-step, must be less than 1 and hence this is impossible.

As for the frequency-dependent interaction, a simplified model of this process is shown in equations (18) and (19).

$$\frac{dB}{dt} = \mu_{max} * (1 - \frac{B}{B_{max}}) * (B - \varphi * B) - \varphi * B \quad (18)$$

$$\frac{dP}{dt} = \varphi * B * \delta - \lambda * P - \gamma * P \qquad (19)$$

With the condition that $\frac{dB}{dt} = 0$ equation (18) can be rewritten as equation (20). This condition must hold in order for there to be a non-zero equilibrium.

$$\varphi = \mu_{max} * (1 - \frac{B}{B_{max}}) * (1 - \varphi) \qquad (20)$$

Using our equilibrium values ($B = 10^9$, $P = 10^5$, $B_{max} = 2.8 \times 10^9$, $\mu_{max} = 1.52$), this is equivalent to equation (21).

$$\varphi = 1.52 * (1 - \varphi) * (1 - \frac{10^9}{2.8*10^9}) \qquad (21)$$

Equation (21) is solved to obtain a value for φ (equations (22) - (25)).

$$\varphi = 0.97 * (1 - \varphi) \qquad (22)$$

$$\varphi = 0.97 - 0.97 * \varphi \qquad (23)$$

$$1.97 * \varphi = 0.97 \qquad (24)$$

$$\varphi = 0.49 \qquad (25)$$

Using our equilibrium values and this value of 0.49 for φ, equation (5) can be rewritten as equation (26).

$$0.49 = 1 - exp\left(-\frac{\lambda * 10^5}{10^9}\right) \qquad (26)$$

Equation (26) is solved to obtain a value for λ (equations (27) - (31)).

$$0.49 = 1 - exp\left(-\frac{\lambda}{10^4}\right) \qquad (27)$$

$$0.51 = exp\left(-\frac{\lambda}{10^4}\right) \qquad (28)$$

$$ln(0.51) = -\frac{\lambda}{10^4} \qquad (29)$$

$$-ln(0.51) * 10^4 = \lambda \qquad (30)$$

$$\lambda \simeq 6733 \qquad (31)$$

Therefore, λ must be approximately equal to 6733 to obtain a non-zero equilibrium as seen in our *in vitro* data with our model fitted values (biologically plausible ones). However, the definition of λ according to equation (4) implies that $\lambda < 1$. Therefore, this is impossible.

316 Even though these analyses rely on a simplified set of equations, using realistic parameter values we
317 have shown that a non-zero equilibrium, as we have seen *in vitro,* cannot be reproduced using models
318 with only a density or frequency-dependent interaction. Instead, phage-bacteria co-existence may be
319 explained by variations in phage predation parameters depending on bacterial resources availability,
320 or bacterial growth rate [14,17–22]. However, to the best of our knowledge a simple mathematical
321 expression linking phage predation to bacterial growth has not yet been developed.

322

323 *Second phage-bacteria interaction: dependence of phage predation on bacterial growth*

324 Here, we consider that a decrease in bacterial growth as bacteria reach stationary phase could firstly
325 affect the phage adsorption rate β, due to changes in receptors on bacterial surfaces, which affect
326 opportunities for phage to bind (Figure 4c). Secondly, this could affect phage production, and thus
327 burst size δ, as phage replication relies on bacterial processes and may decrease when bacterial
328 growth slows down (Figure 4c). Using a single phage predation multiplier, with the same principle of
329 logistic growth applied to bacteria, we allow either or both β and δ to decrease as bacterial growth
330 decreases in our model (equations (32) and (33)).

331 $$\beta = \beta_{max} * \left(1 - \frac{B}{B_{max}}\right) \qquad (32)$$

332 $$\delta = \delta_{max} * \left(1 - \frac{B}{B_{max}}\right) \qquad (33)$$

333 These equations imply that, as bacterial population size increases towards carrying capacity (B_{max}),
334 phage parameters will be reduced (Figure 4d).

335 ## Identification of the best-fitting phage-bacteria interactions to
336 ## reproduce the *in vitro* dynamics

337 Overall, we considered 6 different models, either density- or frequency-dependent, and with either or
338 both the phage adsorption rate and burst size linked to bacterial growth. Note that we did not include
339 a phage decay rate in these models, as this did not affect the dynamics of the system over 24h, for a
340 wide range of decay rates (Figure 5 – figure supplement 1).

341 We used a Bayesian methodology to fit the models simultaneously to the lytic phage and double-
342 resistant progeny numbers from the transduction co-culture datasets with starting phage
343 concentrations of 10^3 and 10^5 pfu/mL (Figure 2), and tested whether the estimated parameters could
344 reproduce the dynamics seen with the starting phage concentration of 10^4 pfu/mL. Convergence and
345 posterior distribution plots for our best-fitting model are shown in Figure 5 – figure supplement 2.

346 All models successfully reproduced the trends seen *in vitro* when the phage were started at either 10^3
347 and 10^4 pfu/mL (Figure 5a-b). However, only the two models where only phage burst size decreases
348 as the bacteria population approaches carrying capacity were able to reproduce the increase in phage
349 numbers seen in the later hours of the 10^5 pfu/mL dataset, despite all models having been fitted to
350 this dataset (Figure 5a-b). This was confirmed by calculating the average Deviance Information Criteria
351 (DIC) value for the models, which favours best-fitting models while penalising more complex models
352 (i.e. with more parameters) [36]. The two models where only phage burst size decreases as the bacteria
353 population approaches carrying capacity had the lowest DIC values, indicating that they were the
354 better-fitting models (Table 1).

355 Our initial experiments considered the dynamics over 24h for varying phage starting concentrations.
356 To test the ability of our model to recreate the dynamics under changing bacterial levels, we replicated
357 our transduction co-culture experiments with starting concentrations of 10^6 cfu/mL bacteria instead
358 of 10^4 cfu/mL, varying the starting phage concentration between 10^4 and 10^6 pfu/mL, and measuring

359 bacteria and phage numbers after 24h of co-culture. We then used the estimated parameter values
360 (Table 1) to try to reproduce these 24h numbers of bacteria and phage.

361 Increasing the starting phage concentration led to an increase in the number of phage after 24h
362 (Figure 5c). For a starting phage concentration between 10^4 and 10^6 pfu/mL, increasing starting phage
363 numbers did not affect single-resistant parents B_E and B_T numbers after 24h, but led to a progressive
364 increase in double-resistant progeny B_{ET} numbers. Increasing starting phage numbers above 10^6
365 pfu/mL caused bacteria numbers after 24h to decrease.

366 Using the estimated parameter values (Table 1) with the model where only burst size is linked to
367 bacterial growth, we see that the density model cannot reproduce these dynamics as it predicts that
368 bacteria become extinct rapidly (Figure 5c). The frequency-dependent model is able to reproduce
369 these trends, but fails to recreate the exact same numbers of phage and bacteria, predicting a decline
370 in bacterial levels when the starting phage concentration increases above 10^5 pfu/mL, a lower
371 threshold than seen in the data (Figure 5c). The same overall trends are seen for the models where
372 only the adsorption rate is linked to bacterial growth, or both adsorption rate and burst size (Figure 5
373 – figure supplement 3).

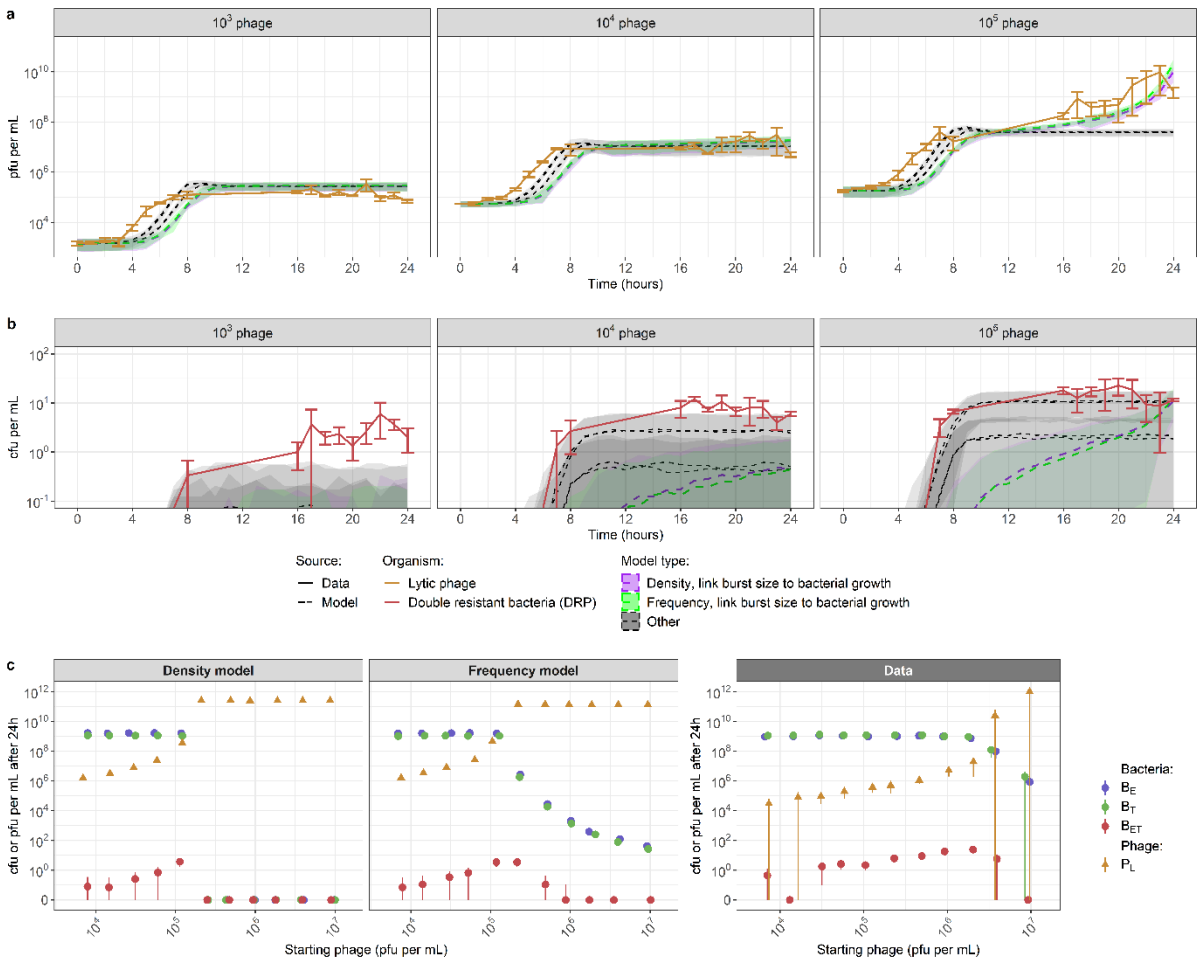

Figure 5: Accuracy of the best-fitted models to reproduce *in vitro* phage-bacteria dynamics. (a-b) The models with only phage burst size linked to bacterial growth are the most accurate to reproduce *in vitro* trends in lytic phage (a) and double resistant bacteria (b) numbers, starting from a bacteria concentration of 10^4 cfu/mL and varying phage concentrations. All models (dashed lines) can reproduce the trends seen *in vitro* when phage are started at 10^3 or 10^4 pfu/mL (data in solid lines), but only the models with just the phage burst size linked to bacterial growth (coloured model output) can reproduce the trend seen when phage are started at 10^5 pfu/mL. Other models (grey) either only have the phage adsorption rate linked to bacterial growth, or both the phage adsorption rate and burst size. Models are fitted to the 10^3 and 10^5 data, and tested with the 10^4 data. Parameter values used are the median fitted values (Table 1). Shaded areas indicate standard deviation generated from Poisson resampling of model results. Error bars for the data (solid lines) indicate mean +/- standard error, from 3 experimental replicates. **(c) When further testing fitted model dynamics starting from**

387 **10^6 cfu/mL bacteria and varying phage concentrations, the density-dependent model incorrectly**
388 **predicts bacterial extinction, while the frequency-dependent model reproduces the trend, but not**
389 **the exact values of the 24h data.** In the co-culture used to generate the data, each single-resistant
390 parent strain (B_E and B_T) is added at a starting concentration of 10^6 cfu/mL, and no double-resistant
391 progeny (B_{ET}) are initially present. The starting concentration of lytic phage (P_L) varies (x axis). Points
392 indicate mean results, and are each slightly shifted horizontally to facilitate viewing. Error bars indicate
393 either mean +/- standard deviation for the models (left/centre panels), or mean +/- standard error for
394 the data (right panel). Parameter values used are the median fitted values (Table 1). **Figure**
395 **supplement 1: Model results are not affected by phage decay rate over a wide range of values.**
396 Previous estimates of phage decay rate per hour are between 10^{-3} *in vitro* and up to 10^{-1} *in vivo* [38].
397 **Figure supplement 2: Convergence and posterior distributions for the best-fitting model.** (a-d)
398 Parameter convergence plots. Fitting was performed using two chains (black and red). (e-h) Posterior
399 distributions. The prior distributions for the burst size and latent period are shown in blue. The prior
400 distributions for other parameters were uninformative and not shown. **Figure supplement 3: Model**
401 **performance in reproducing the 24h data values for different starting concentrations of phage with**
402 **different links between phage predation and bacterial growth rate.** (a) Phage adsorption rate
403 decreases as bacterial growth rate decreases. (b) Phage burst size and adsorption rate decrease as
404 bacterial growth rate decreases.

405 **Table 1: Estimated parameter values from fitting to *in vitro* data.** Values show median and 95% credible intervals for posterior distributions. Parameter units
406 are indicated in parentheses. Fitting was performed using the Markov chain Monte Carlo Metropolis–Hastings algorithm and the data from the co-culture
407 with a starting bacterial concentration of 10^4 cfu/ml and phage concentration of 10^3 and 10^5 pfu/ml. DIC: Deviance Information Criteria. A smaller DIC
408 indicates better model fit. DIC values are relative to the smallest DIC calculated, which is for the frequency-dependent model with only burst size linked to
409 bacterial growth (line 5, parameters in bold).

Interaction type	**Adsorption rate linked to growth**	**Burst size linked to growth**	**Adsorption rate β (phage^{-1} bacteria^{-1} hour^{-1})**	**Burst size δ (phage)**	**Transducing phage proportion α (proportion of burst size)**	**Phage latent period τ (hour)**	**DIC**
Density dependent	**Yes**	**No**	4.5×10^{-9} (4.1×10^{-9} ; 5.0×10^{-9})	12 (10 ; 14)	3.1×10^{-8} (1.5×10^{-8} ; 5.8×10^{-8})	0.64 (0.55 ; 0.73)	610
	No	**Yes**	1.6×10^{-10} (1.5×10^{-10} ; 1.7×10^{-10})	79 (72 ; 86)	1.4×10^{-8} (1.1×10^{-8} ; 1.7×10^{-8})	0.65 (0.62 ; 0.69)	63
	Yes	**Yes**	4.3×10^{-9} (3.9×10^{-9} ; 4.6×10^{-9})	43 (37 ; 49)	1.2×10^{-8} (6.4×10^{-9} ; 2.3×10^{-8})	0.93 (0.86 ; 0.99)	298
Frequency dependent	**Yes**	**No**	5.1×10^{-9} (3.7×10^{-9} ; 6.7×10^{-9})	10 (8 ; 12)	3.1×10^{-7} (2.3×10^{-7} ; 4.3×10^{-7})	0.60 (0.50 ; 0.69)	680
	No	**Yes**	**2.3×10^{-10} (2.1×10^{-10} ; 2.4×10^{-10})**	**76 (70 ; 83)**	**1.0×10^{-8} (8.5×10^{-9} ; 1.4×10^{-8})**	**0.72 (0.69 ; 0.77)**	**0**
	Yes	**Yes**	4.7×10^{-9} (3.8×10^{-9} ; 5.8×10^{-9})	31 (26 ; 37)	1.7×10^{-7} (1.3×10^{-7} ; 2.1×10^{-7})	0.88 (0.79 ; 0.96)	370

410

411 ## Analysis of phage predation and transduction dynamics

412 Parameter estimates for our best-fitting model (with a frequency-dependent interaction and a link
413 between phage burst size and bacterial growth only) suggest that the adsorption rate is 2.3 x 10^{-10}
414 (95% credible interval: 2.1 x 10^{-10} - 2.4 x 10^{-10}) which is the smallest estimate from the models (Table
415 1). On the other hand, the estimated burst size is relatively large at 76 (70 - 83) phage, and is higher
416 than a previous *in vitro* estimate for 80α of 40 [37]. However, due to the decrease in burst size when
417 bacteria are in stationary phase, we expect that this number would change depending on the
418 conditions under which it is measured (Figure 6a). Finally, the estimated latent period of 0.72h (0.69 -
419 0.77) is slightly longer than a previous in vitro estimate of 0.67h [37]. Regarding the other models, we
420 note some biologically unlikely parameter estimates which further suggest that these models are
421 inappropriate, such as the low burst size for the models with only the adsorption rate linked to
422 bacterial growth (12 (10 - 14) and 10 (8 - 12)), or the high latent period for the models with both
423 adsorption rate and burst size linked to bacterial growth (0.93 (0.86 - 0.99) and 0.88 (0.79 - 0.96))
424 (Table 1).

425 We used our best-fitting model to reproduce our *in vitro* data (Figure 2) and uncover the underlying
426 phage-bacteria dynamics. Due to the link between phage burst size and bacterial growth, burst size
427 decreases as bacteria reach carrying capacity after 8h (Figure 6a-b). This is reflected in the relative
428 change in phage numbers, which tends towards 0 after 8h (Figure 6b). After this point, phage incidence
429 remains stable for the 10^3 and 10^4 pfu/mL dataset, but starts increasing again significantly after 20h
430 for the 10^5 pfu/mL dataset as bacteria numbers start decreasing due to phage predation, allowing
431 burst size to increase again (Figure 6a-c).

432 We estimate that for every 10^8 new lytic phage released during burst, there was approximately one
433 transducing phage carrying an antibiotic resistance gene (Table 1, Figure 6c). Note that new double-
434 resistant progeny (DRP) can either be generated by transduction, or by replication of already existing
435 DRP. Using the model, we found that DRP were always predominantly generated by transduction

436 rather than by growth (Figure 6d). This is because DRP only appear after 2 to 4h, while after 4h

437 bacterial growth rate starts decreasing as the total bacteria population approaches carrying capacity

438 (Figure 6b&d).

439

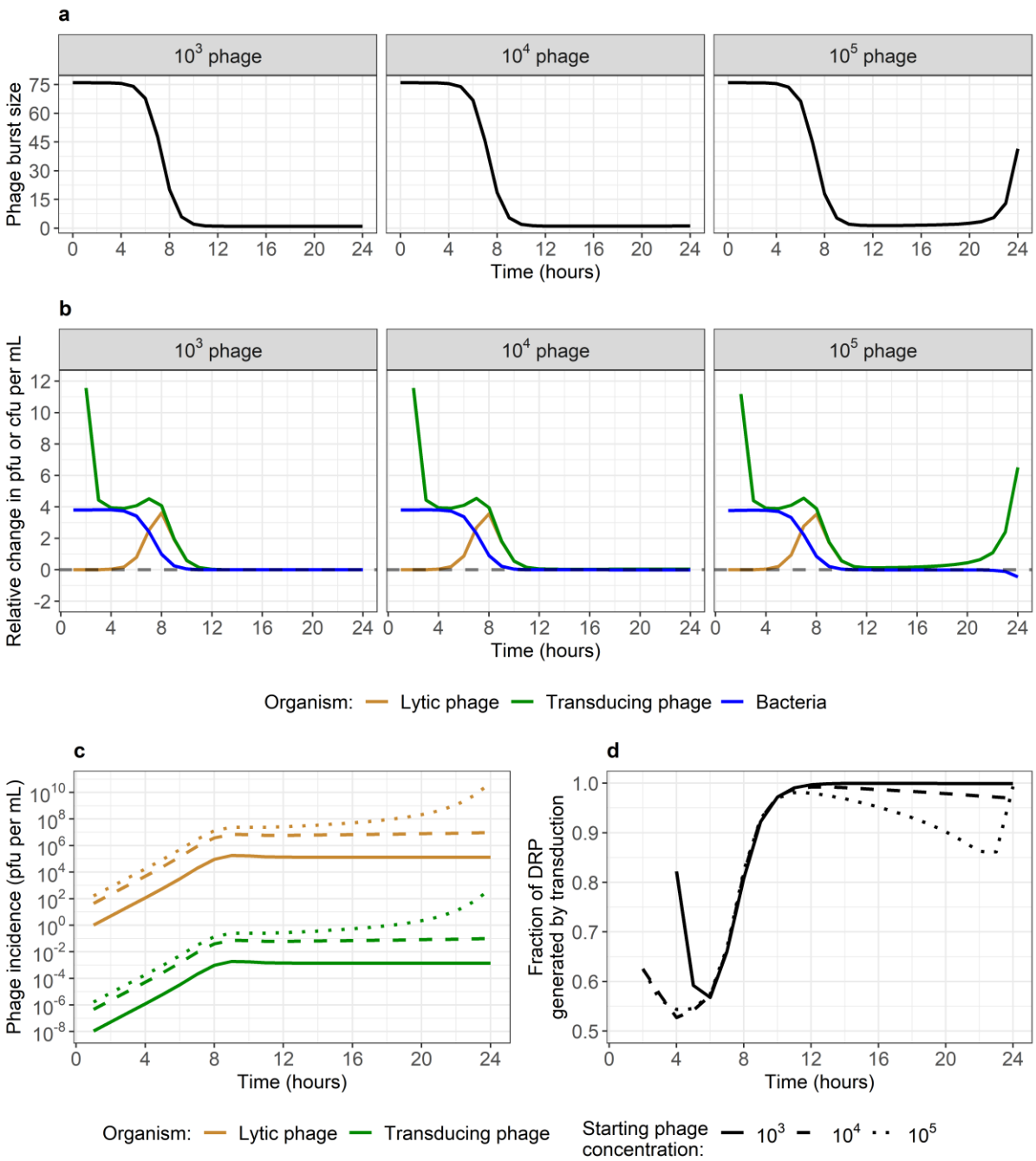

440

441 **Figure 6: Underlying phage and bacteria dynamics generated by the best-fitting frequency-**

442 **dependent model with burst size linked to bacterial growth.** Model parameters are the median

443 estimates from model fitting (Table 1). **(a) Phage burst size over time, by starting phage**
444 **concentration.** As bacteria reach stationary phase after 8h, phage burst size decreases. In the 10^5
445 dataset, we see that burst size is predicted to increase again after 20h. This is due to bacterial numbers
446 decreasing as bacteria are being lysed by phage. **(b) Relative change in phage and bacteria numbers**
447 **over time, by starting phage concentration.** The number of new phage generated at each time step
448 increases (positive value) until bacteria reach stationary phase around 8h. This applies to lytic and
449 transducing phage. In the 10^5 dataset, phage keep increasing after 10h, eventually causing a decrease
450 in bacterial numbers (negative value), which translates into a further acceleration in the increase in
451 phage numbers due to the increased burst size (Figure 5a). After 8h, the relative changes in lytic and
452 transducing phage numbers are identical. **(c) Incidence of lytic (gold) and transducing (green) phage**
453 **over time, by starting phage concentration (linetype).** For any dataset and time-point, there is
454 approximately 1 new transducing phage generated for each 10^8 new lytic phage. **(d) Fraction of**
455 **double-resistant progeny (DRP) generated by transduction each hour over time, by starting phage**
456 **concentration (linetype).** DRP generation always occurs predominantly by transduction, rather than
457 by growth of already existing DRP. Note that the time at which DRP are first generated varies by
458 starting phage concentration.

Discussion

We observed rapid *in vitro* horizontal gene transfer of antimicrobial resistance (AMR) by generalised transduction in *Staphylococcus aureus*, alongside equilibriums in phage and bacteria numbers which varied depending on the starting number of phage. The most accurate mathematical model to replicate phage-bacteria dynamics, including generalised transduction, represented phage predation as a frequency-dependent interaction, and linked phage burst size to bacterial growth. To the best of our knowledge, these two elements have both been suggested previously [17,18,34], yet never combined.

Density-dependent models have been compared to data at less fine time scales (e.g. daily time points) or over smaller time periods (e.g. less than 8h), where they were able to reproduce *in vitro* values from experiments in chemostats, and have been helpful to improve our basic understanding of phage-bacteria dynamics [14–16]. However, here we show that this type of interaction is not able to reproduce finer hourly dynamics, and does not perform consistently when varying concentrations of starting phage and bacteria. Using this, alongside a critique of the mathematical implications of this process, we argue that density-dependence is not a biologically accurate representation of phage predation, as it fails to reproduce these dynamics at high or low numbers of phage and bacteria, which would correspond to scenarios potentially seen during phage therapy.

Our work adds to the growing body of evidence that phage predation depends on bacterial growth [14,17–23]. This has implications for antibiotic-phage combination therapy, as it suggests that bacteriostatic antibiotics, which prevent bacterial growth, could reduce phage predation. This effect has been previously seen in *S. aureus* [38]. In the environment, including in persistent infections, bacteria spend most of their time in stationary phase [39]. This suggests that bacteria and phage may be able to co-exist for prolonged periods of time in a broad range of settings, without the phage systematically eradicating the bacteria. Under such conditions, phage may mediate horizontal gene transfer by transduction between bacteria at relatively low levels, but for prolonged periods of time. This may be

483 particularly relevant for *S. aureus*, since approximately 20% of humans are colonised asymptomatically
484 by this bacterium at any given time [40], and at least 50% of these carriers may also carry phage capable
485 of generalised transduction [41], suggesting a constant background evolution rate for *S. aureus* in the
486 human population. Combined with environmental exposure to antibiotics which acts as a selective
487 pressure, this may contribute to the risk of multidrug resistant bacteria evolution.

488 Our experimental design is both a strength and a limitation of our study. Since we jointly designed the
489 experiments and models, we are confident that we have included in our mathematical model all the
490 organisms and interactions present *in vitro*. We are therefore confident in the conclusions on model
491 structure, however, the usage of such a specific experimental system with two bacterial strains of the
492 same genetic background and one phage limits the generalisability of our parameter values, as these
493 will likely vary for different bacteria and phage. Growth conditions will likely also differ between the
494 *in vitro* environment studied here, and *in vivo* conditions. Here, our model assumes that phage do not
495 decay, that bacteria do not become resistant to phage, and that they can grow indefinitely as they are
496 observed in a rich medium for 24h only, but over longer periods of time it may be necessary to revisit
497 these assumptions [42]. Finally, we assumed that the proportion of transducing phage created was
498 independent of the gene being transduced (*ermB*, on the bacterial chromosome, or *tetK*, on a
499 plasmid). This was supported by preliminary work (not shown), but should be further investigated to
500 improve our understanding of the factors that can facilitate or prevent transduction of different genes.
501 To answer all of these questions, future work should investigate both phage predation and
502 transduction dynamics over longer time periods, with different strains of bacteria and phage.

503 All our models captured certain aspects of the trends seen *in vitro*, but also underestimated phage
504 numbers between 5-7h by up to 20 times. This is likely a consequence of our experimental design. To
505 count lytic phage, we centrifuged and filtered the co-culture to remove bacteria. This could have
506 caused the premature burst of some phage-infected bacteria, artificially increasing the numbers of
507 phage we then counted [43]. Since the period between 5-7h is when phage infections are highest (Figure
508 6b), this is why we would see such a large discrepancy at this stage. We also note that the models with

509 only phage burst size linked to bacterial growth underestimated the number of double-resistant
510 progeny (DRP). This small difference (up to 10 cfu/mL) is likely due to our choice of using a
511 deterministic model. This type of model is useful for our purpose of fitting to *in vitro* data and analysing
512 the underlying dynamics here, but mathematically allows for fractions of bacteria to exist, instead of
513 just whole numbers. Future analyses using a stochastic model would better capture random effects,
514 which can have an important impact at low numbers.

515 Multiplicity of infection (MOI, starting ratio of phage to bacteria) is a commonly used metric to present
516 results of experiments with these organisms [32]. With a starting concentration of 10^4 bacteria per mL,
517 we were able to fit our model to the dynamics for two MOI (0.1 and 10), and replicate those of a third
518 (1). However, when trying to use the same model for these same three MOI, but with a starting
519 bacterial concentration to 10^6, we found differences between our model and values seen after 24h.
520 This indicates that MOI is not appropriate to summarise all the complexity of the underlying phage-
521 bacteria dynamics. Future experimental studies should express their results as a function of their
522 starting concentration of phage and bacteria, not just MOI.

523 In any case, the failure of our model to replicate 24h values with a different starting bacteria
524 concentrations shows that, whilst we have reduced the model structure uncertainty, we are still not
525 fully capturing the phage-bacteria interaction. Currently, our model predicts that, for a starting
526 concentration of 10^6 bacteria, a starting concentration of 10^5 phage or more will be enough to cause
527 a decrease in bacterial numbers after 24h, while our data shows that the starting concentration of
528 phage must be higher than 10^6 for this to happen. *In vitro*, it is likely that slower bacterial growth
529 simultaneously affects the phage adsorption rate, latent period and burst size, each to varying extents
530 [14,17–23]. This would explain why we would need a higher starting concentration of phage for a higher
531 starting concentration of bacteria, to exert a strong enough predation pressure before bacteria reach
532 stationary phase, causing a reduction in phage predation. However, here we have only made the first
533 step in this process, having linked the burst size linearly to the bacterial growth rate, instead of trying
534 to link different phage predation parameters to bacterial growth using different functions. These

complexities need to be explored further, supported by i*n vitro* work measuring phage predation parameters at various time points. In *S. aureus*, wall teichoic acid (WTA) is the phage receptor [44,45]. Lack of WTA glycosylation has been shown to induce phage resistance [46], and changes in WTA structure at different growth phases may be possible, since one of the genes involved in its synthesis is repressed by a quorum sensing system [47]. However, to the best of our knowledge this has not yet been investigated.

Despite being recognised as a major mechanism of horizontal gene transfer, thus far there have been limited mathematical modelling studies on the dynamics of transduction of AMR [13]. Using our model, we are able to estimate numbers of transducing phage which we cannot count *in vitro*, and see that approximately 1 generalised transducing phage is generated per 10^8 lytic phage, consistent with previous estimates [48,49]. Here, we show that this number, which may seem insignificant, is enough to consistently lead to the successful horizontal gene transfer of AMR, resulting in DRP after only 7h, substantially less than the usual duration of antibiotic treatment. We also show that transduction is the dominant mechanism to create new DRP throughout the entire experiment, rather than growth of existing DRP. This echoes the conclusions of previously published work on the importance of transduction, including *in vivo* experiments and with other *Staphylococcus* species [6,7,29,50].

Our findings suggest that transduction is currently under-emphasised in the exploration of phage-bacteria dynamics. Future studies on this topic should not assume that transduction can be dismissed by default, but instead investigate whether it is relevant in their system. This requires further *in vitro* and *in vivo* monitoring to identify scenarios where transduction plays a significant role in the transfer of AMR genes, likely depending on the environment, and characteristics of the bacteria and phage present. This will require new experimental designs, since counting phage numbers can be difficult, notably with clinical strains of bacteria. This should also be investigated in the presence of antibiotics, where the importance of selection enters, increasing the fitness of the small numbers of DRP generated by transduction.

560 In conclusion, the dual nature of phage (predation and transduction) leads to complex interactions
561 with bacteria. These dynamics must be clarified, to correctly evaluate the extent to which phage
562 contribute to the global spread of AMR. We must also understand this dual nature to guarantee a safe
563 design of phage therapy. Otherwise, ignoring transduction may lead to worse health outcomes in
564 patients if phage contribute to spreading AMR instead of overcoming it. Interdisciplinary work will be
565 essential to answer these urgent public health questions in the near future.

566 # Materials and Methods

567 All analyses were conducted using the statistical software R [51]. The underlying code and data are
568 available in a GitHub repository: https://github.com/qleclerc/mrsa_phage_dynamics.

569 ## Experimental methods

570 *Strains and phage used*

571 The *Staphylococcus aureus* parent strains used for our transduction experiment were obtained from
572 the Nebraska Transposon Mutant Library [52]. These were strain NE327, carrying the *ermB* gene
573 encoding erythromycin resistance and knocking out the ϕ3 integrase gene, and strain NE201KT7, a
574 modified NE201 strain with a kanamycin resistance cassette instead of the *ermB* gene knocking out
575 the ϕ2 integrase gene, and a pT181 plasmid carrying the *tetK* gene encoding tetracycline resistance [53].
576 Growing these strains together in identical conditions as our co-culture below, but without the
577 addition of exogenous phage, does not lead to detectable horizontal gene transfer (HGT; data not
578 shown). To enable HGT, exogenous 80α phage was used, a well-characterised temperate phage of *S.*
579 *aureus* capable of generalised transduction [33]. To count lytic phage, *S. aureus* strain RN4220 was used,
580 a restriction deficient strain highly susceptible to phage infection [54].

581

582 *Transduction co-culture protocol*

583 Pre-cultures of NE327 and NE201KT7 were prepared separately in 50mL conical tubes with 10mL of
584 Brain Heart Infusion Broth (BHIB, Sigma, UK), and incubated overnight in a shaking water bath (37°C,
585 90rpm). The optical densities of the pre-cultures were checked at 625nm the next day to confirm
586 growth. The pre-cultures were diluted in phosphate-buffered saline (PBS), and added to a glass bottle
587 of fresh BHIB to reach the desired starting concentration in colony forming units per mL (cfu/mL) for

588 each strain, forming a master mix for the co-culture. $CaCl_2$ was added at a concentration of 10mM to
589 the master mix. Phage 80α stock was diluted in phage buffer (50 mM Tris-HCl pH 7.8, 1 mM MgSO4,
590 4 mM CaCl2 and 1 g/L gelatin; Sigma–Aldrich), and added to the master mix to reach the desired
591 starting concentration in plaque forming units per mL (pfu/mL). Ten 50mL conical tubes were prepared
592 (one co-culture tube for each timepoint, from 0 to 8h and 16 to 24h), each with 10mL from the master
593 mix. Each co-culture tube was then incubated in a shaking water bath (37°C, 90rpm) for the
594 corresponding duration.

595 Bacteria counts for each timepoint were obtained by diluting the co-culture in PBS before plating 50µL
596 on selective agar, either plain Brain Heart Infusion Agar (BHIA, Sigma, UK), BHIA with erythromycin
597 (Sigma, UK) at 10mg/L, BHIA with tetracycline (Sigma, UK) at 5mg/L, or BHIA with both erythromycin
598 and tetracycline (10mg/L and 5mg/L respectfully). Note we plated 500µL instead of 50 on the plates
599 with both antibiotics, to increase the sensitivity of the assay. This allowed distinction between each
600 parent strain, resistant to either erythromycin or tetracycline, and the double resistant progeny (DRP)
601 generated by transduction. Plates were then incubated at 37°C for 24h, or 48h for plates containing
602 both antibiotics. Colonies were counted on the plates to derive the cfu/mL in the co-culture for that
603 timepoint.

604 Lytic phage counts for each timepoint were obtained using the agar overlay technique [55]. Briefly, the
605 co-culture was centrifuged at 4000rpm for 15 minutes, filtered twice with 10µm filters, and diluted in
606 Nutrient Broth No. 2 (NB2, ThermoFisher Scientific, UK). 15mL conical tubes were prepared with 300µl
607 of RN4220 grown overnight in NB2, and $CaCl_2$ at a concentration of 10mM. 200µl of diluted phage
608 were added, and the tubes were left to rest on the bench for 30 minutes. The contents of the tubes
609 were then mixed with 7mL of phage top agar, and poured on phage agar plates. Phage agar was
610 prepared using NB2, supplemented with agar (Sigma, UK) at 3.5g/L for top agar and 7g/L for plates.
611 The plates were incubated overnight at 37°C. Clear spots in the bacterial lawn were counted to derive
612 the pfu/mL in the co-culture for that timepoint.

613 *Polymerase chain reaction protocols*

614 To confirm that DRP contained both the *ermB* and *tetK* genes, primers ermBF (5'-
615 CGTAACTGCCATTGAAATAGACC-3'), ermBR (5'-AGCAAACTCGTATTCCACGA-3'), tetKF

616 (5'-ATCTGCTGCATTCCCTTCAC-3'), and tetKR (5'-GCAAACTCATTCCAGAAGCA-3') were used. Strains
617 NE327 (only containing *ermB*) and NE201KT7 (only containing *tetK*) were used as positive and negative
618 controls.

619 To confirm that 80α lysogeny did not occur in our co-culture, we applied a previously published
620 method [33] and used a combination of four primers: SaRpmF (5'-GACTGAATGCCCAAACTGTG-3') in the
621 *S. aureus rpmF* gene, SMT178 (5'-GGCTGGGAATTAATGGAAGATG-3') in the 80α integrase, SaSirH (5'-
622 TTAAGTAGCATCGTTGCATTCG-3') in the *S. aureus sirH* gene, and SMT179 (5'-
623 GAGTCCTGTTTGCGAATTAGG-3') in the 80α ORF73 region. SaRpmF and SMT178 were used to amplify
624 the left prophage junction (*attL*), SaSirH and SMT179 to amplify the right junction (*attR*), and SaRpmF
625 and SaSirH to amplify the bacterial insertion site (*attB*). RN4220 was used as a negative control for
626 lysogeny, and JP8488, an RN4220 strain lysogenic for 80α, was used as a positive control (obtained
627 from José Penadés and Nuria Quiles, Imperial College London).

628 All PCRs were conducted using OneTaq Hot Start Quick-Load 2X Master-mix, following the
629 manufacturer's protocol. Tested samples were homogenised in 20µl nuclease-free water, and 1.5µl of
630 each suspension was used as template for a total reaction volume of 25µl.

631

632 # Mathematical modelling methods

633 *General model structure*

634 We designed a deterministic, compartmental model to replicate our experimental conditions. We
635 included 6 populations: B_E (corresponding to ery-resistant NE327), B_T (tet-resistant NE201KT7), B_{ET}

(double resistant progeny, DRP), P_L (lytic phage), P_E (phage transducing *ermB*) and P_T (phage transducing *tetK*). Their interactions are represented in Figure 2.

Bacteria from each strain θ ($\theta \in \{E, T, ET\}$) can multiply at each time step *t* following logistic growth at rate μ_θ, with a maximum value $\mu_{max\theta}$ which declines as the total bacteria population N (= $B_E + B_T + B_{ET}$) approaches carrying capacity N_{max}.

$$\mu_\theta = \mu_{max_\theta} * (1 - \frac{N}{N_{max}}) \qquad (34)$$

At each time step *t*, a proportion λ of lytic phage (P_L) infect a number of bacteria (φ_L), replicate, and burst out from the bacteria with a burst size $\delta + 1$ after a latent period τ. During phage replication, a proportion α of new phage are transducing phage. The nature of the transducing phage (P_E or P_T) depends on the bacteria being infected (e.g. B_E bacteria can only lead to P_E phage). Then, a proportion λ of these transducing phage (P_E or P_T) infect a number of bacteria (φ_E or φ_T). If they successfully infect a bacterium carrying the other resistance gene (e.g. P_E phage infecting a B_T bacterium), this creates double resistant progeny (B_{ET}). The complete model equations can be found below.

$$\frac{dB_E}{dt} = \mu_E * (B_E - \omega * \left((\varphi_L + \varphi_T) * \frac{B_E}{N}\right)) - (\varphi_L + \varphi_T) * \frac{B_E}{N} \qquad (35)$$

{Change in B_E = growth of B_E – infections by P_L – infections by P_T}

$$\frac{dB_T}{dt} = \mu_T * (B_T - \omega * \left((\varphi_L + \varphi_E) * \frac{B_T}{N}\right)) - (\varphi_L + \varphi_E) * \frac{B_T}{N} \qquad (36)$$

{Change in B_T = growth of B_T – infections by P_L – infections by P_E}

$$\frac{dB_{ET}}{dt} = \mu_{ET} * (B_{ET} - \omega * \left(\varphi_L * \frac{B_{ET}}{N}\right)) - \varphi_L * \frac{B_{ET}}{N} + \varphi_E * \frac{B_T}{N} + \varphi_T * \frac{B_E}{N} \qquad (37)$$

{Change in B_{ET} = growth of B_{ET} – infections by P_L + infections of B_T by P_E + infections of B_E by P_T}

$$\frac{dP_L}{dt} = \varphi_L(t - \tau) * \delta * \left(1 - \alpha * \frac{B_E + B_T + 2 * B_{ET}}{N}\right) - \lambda * P_L \qquad (38)$$

{Change in P_L = new P_L phage – P_L phage infecting bacteria}

$$\frac{dP_E}{dt} = \varphi_L(t-\tau) * \delta * \alpha * \frac{B_E+B_{ET}}{N} - \lambda * P_E \qquad (39)$$

{Change in P_E = new P_E phage – P_E phage infecting bacteria}

$$\frac{dP_T}{dt} = \varphi_L(t-\tau) * \delta * \alpha * \frac{B_T+B_{ET}}{N} - \lambda * P_T \qquad (40)$$

{Change in P_T = new P_T phage – P_T phage infecting bacteria}

Some parameters (τ, α, ω) are constant, while others (μ_E, μ_T, μ_{ET}, β, φ_L, φ_E, φ_T, δ) can change at each time step and depending on the specified interaction mechanism. Note that ω is a special parameter equal to 0 if the model is density-dependent, or 1 if it is frequency-dependent.

Density-dependent interaction

Over one time step, both the number of phage infecting bacteria and the number of bacteria infected by phage are equal to the product of the number of phage, bacteria, and phage adsorption rate. In our equations for density-dependence, given the phage adsorption rate β, the proportion λ of phage that infect any bacteria is:

$$\lambda = \beta * N \qquad (41)$$

And the number of bacteria infected by a phage θ ($\theta \in \{L, E, T\}$) is:

$$\varphi_\theta = \lambda * P_\theta \qquad (42)$$

Note that the parameter ω is set to 0 in this case.

Frequency-dependent interaction

Using this interaction prevents the number of phage infecting bacteria over one time step to be higher than the total number of phage in the system (and the number of bacteria being infected one time step to be higher than the total number of bacteria in the system). Equations (41) and (42) then become:

$$\lambda = (1 - exp\,(-\beta * N)\,) \qquad (43)$$

$$\varphi_\theta = \left(1 - exp\,\left(-\lambda * \frac{P_\theta}{N}\right)\right) * N \qquad (44)$$

With the frequency-dependent interaction, we set the parameter ω to 1. This ensures that, over one time step and for any bacterium, phage infection and bacteria replication are mutually exclusive events. Without this modification, phage infections would not be able to reduce bacterial population size due to mathematical constraints. Equation (45) shows a simplified frequency-dependent model for a single bacterial strain *B*, without any correction term.

$$\frac{dB}{dt} = \mu_{max} * (1 - \frac{B}{B_{max}}) * B - \varphi_\theta * B \quad (4445$$

According to equation (45), the change in bacterial numbers depends on the relative values of bacterial growth and bacterial death due to phage predation, expressed in equation (46).

$$\mu_{max} * (1 - \frac{B}{B_{max}}) - \varphi \qquad (46)$$

The necessity for a correction term on the left hand side of equation (45) arises from the maximum values of μ_{max} and φ_θ. As can be deduced from equation (44), the maximum possible value for φ_θ is 1. According to our fitted parameter values, the maximum value for μ_{max} in our model is approximately 1.5, and the carrying capacity B_{max} is approximately 2.8 x 10^9. Substituting these into equation (46) leads to equation (47).

$$1.5 * (1 - \frac{B}{2.8*10^9}) - 1 \qquad (47)$$

To have a decline in the bacterial population, we must therefore satisfy the condition stated in equation (48).

$$1.5 * (1 - \frac{B}{2.8*10^9}) < 1 \qquad (48)$$

This can be rearranged into equation (49) by dividing by 1.5.

$$1 - \frac{B}{2.8*10^9} < \frac{1}{1.5} \qquad (49)$$

Finally, by subtracting 1 and multiplying by -2.8 x 10^9, we obtain equation (50).

$$\mathrm{B} > -(\frac{1}{1.5} - 1) * 2.8 * 10^9 \qquad (50)$$

Solving equation (50) leads to the condition that the number of bacteria must be greater than 9.3 x 10^8 in order for bacterial growth to be low enough that bacteria numbers decrease. In other words, it is impossible for the effect of phage predation to decrease bacteria numbers below 9.3 x 10^8. We overcome this by applying a correction term to equation S1, leading to equation (51).

$$\frac{d\mathrm{B}}{dt} = \mu_{max} * (1 - \frac{B}{B_{max}}) * (B - \varphi_\theta * B) - \varphi_\theta * B \qquad (51)$$

This is equivalent to saying that bacteria infected by phage cannot replicate and hence is more biologically realistic.

Link between bacterial growth and phage predation

We consider that reduced bacterial growth can lead to decreased phage predation, through reduced adsorption (β) and/or burst size (δ). Equations (52) and (53) allow these parameters to decrease as bacterial growth decreases, using the same principle of logistic growth as seen in equation (34).

$$\beta = \beta_{max} * \left(1 - \frac{N}{\mathrm{N}_{max}}\right) \qquad (52)$$

$$\delta = \delta_{max} * \left(1 - \frac{N}{\mathrm{N}_{max}}\right) \qquad (53)$$

If we do not link these parameters to bacterial growth, we assign them their maximum values.

$$\beta = \beta_{max} \qquad (54)$$

$$\delta = \delta_{max} \qquad (55)$$

721 *Model fitting*

722 We fit our model to the *in vitro* data using the Markov chain Monte Carlo Metropolis–Hastings
723 algorithm. For every iteration, this algorithm slightly changes the parameter values, runs the model,
724 assesses the resulting model fit to the data, and accepts or rejects these new parameter values based
725 on whether the model fit is better or worse than with the previous set of values. We run the algorithm
726 with two chains, and once convergence has been reached (determined using the Gelman-Rubin
727 diagnostic, once the multivariate potential scale reduction factor is less than 1.2 [56]), we generate
728 50,000 samples from the posterior distributions for each parameter.

729 In a first instance, we used our growth co-culture data, where phage are absent, to calibrate the
730 bacterial growth rate parameters $\mu_{max\theta}$ for each bacteria strain θ ($\theta \in \{E, T, ET\}$), as well as the carrying
731 capacity N_{max} using a simple logistic growth model (equation (9)). All other parameters related to
732 phage predation were set to 0.

733 The phage predation parameters (τ, α, β_{max}, δ_{max}) were jointly estimated by fitting to the phage and
734 double resistant bacteria numbers from the transduction co-culture data. Fitting was performed by
735 evaluating the log-likelihood of each *in vitro* data point being observed in a Poisson distribution, with
736 the corresponding model data point as a mean.

737 To mirror our experimental sampling variation, *in vitro* data points were scaled down to be between
738 1 and 100 before fitting, with the same correction applied to the corresponding model-predicted value
739 for the same timepoint. For example, if at 1h there are 1.4×10^4 phage *in vitro*, this is scaled down to
740 14, and if the corresponding model value is 5.3×10^6, this is scaled down by the same magnitude (i.e.
741 10^3), resulting in a value of 5300.

742 Previous research estimated that the latent period for 80α in *S. aureus* was approximately 40mins
743 (0.67h), and that the burst size was approximately 40 phage per bacterium [37]. Since this study did not
744 provide error values for these point estimates, we assumed the standard deviation and chose the

following informative priors for these parameters: τ ~ *Normal(0.67, 0.07)* (95% confidence interval: 0.53-0.81) and δ_{max} ~ *Normal(40, 7)* (95% confidence interval: 54-26). Due to a lack of available data, we used uninformative priors for the remaining parameters: α ~ *Uniform(0, 1)* and β_{max} ~ *Uniform(0, 1)*.

Acknowledgments

Q.J.L and J.W. were supported by a studentship from the Medical Research Council Intercollegiate Doctoral Training Program (MR/N013638/1). A.G. and G.M.K were supported by grants from the Medical Research Council (MR/P028322/1 and MR/P014658/1 respectively). We would like to thank José Penadés and Nuria Quiles for providing the JP8488 *S. aureus* strain.

Competing interests

The authors declare no competing interests.

References

1. Laxminarayan, R. *et al.* Antibiotic resistance—the need for global solutions. *Lancet Infect. Dis.* **13**, 1057–1098 (2013).
2. Levin, B. R. & Bull, J. J. Population and evolutionary dynamics of phage therapy. *Nat. Rev. Microbiol.* **2**, 166–173 (2004).
3. Clokie, M. R. J., Millard, A. D., Letarov, A. V. & Heaphy, S. Phages in nature. *Bacteriophage* **1**, 31–45 (2011).

765 4. von Wintersdorff, C. J. H. *et al.* Dissemination of Antimicrobial Resistance in Microbial
766 Ecosystems through Horizontal Gene Transfer. *Front. Microbiol.* **7**, (2016).
767 5. Fernández, L., Rodríguez, A. & García, P. Phage or foe: an insight into the impact of viral
768 predation on microbial communities. *ISME J.* **12**, 1171–1179 (2018).
769 6. McCarthy, A. J. *et al.* Extensive Horizontal Gene Transfer during Staphylococcus aureus Co-
770 colonization In Vivo. *Genome Biol. Evol.* **6**, 2697–2708 (2014).
771 7. Haaber, J., Penadés, J. R. & Ingmer, H. Transfer of Antibiotic Resistance in Staphylococcus
772 aureus. *Trends Microbiol.* **25**, 893–905 (2017).
773 8. Balcázar, J. L. How do bacteriophages promote antibiotic resistance in the environment? *Clin.*
774 *Microbiol. Infect.* **24**, 447–449 (2018).
775 9. Verheust, C., Pauwels, K., Mahillon, J., Helinski, D. R. & Herman, P. Contained use of
776 Bacteriophages: Risk Assessment and Biosafety Recommendations. *Appl. Biosaf.* **15**, 32–44
777 (2010).
778 10. Jassim, S. A. A. & Limoges, R. G. Natural solution to antibiotic resistance: bacteriophages 'The
779 Living Drugs'. *World J. Microbiol. Biotechnol.* **30**, 2153–2170 (2014).
780 11. Hassan, A. Y., Lin, J. T., Ricker, N. & Anany, H. The Age of Phage: Friend or Foe in the New Dawn
781 of Therapeutic and Biocontrol Applications? *Pharmaceuticals* **14**, 199 (2021).
782 12. Raj, J. R. M. & Karunasagar, I. Phages amid antimicrobial resistance. *Crit. Rev. Microbiol.* **45**, 701–
783 711 (2019).
784 13. Leclerc, Q. J., Lindsay, J. A. & Knight, G. M. Mathematical modelling to study the horizontal
785 transfer of antimicrobial resistance genes in bacteria: current state of the field and
786 recommendations. *J. R. Soc. Interface* **16**, 20190260 (2019).
787 14. Krysiak-Baltyn, K., Martin, G. J. O., Stickland, A. D., Scales, P. J. & Gras, S. L. Computational
788 models of populations of bacteria and lytic phage. *Crit. Rev. Microbiol.* **42**, 942–968 (2016).
789 15. Campbell, A. Conditions for the Existence of Bacteriophage. *Evolution* **15**, 153–165 (1961).
790 16. Levin, B. R., Stewart, F. M. & Chao, L. Resource-Limited Growth, Competition, and Predation: A

791 Model and Experimental Studies with Bacteria and Bacteriophage. *Am. Nat.* **111**, 3–24 (1977).

792 17. Weld, R. J., Butts, C. & Heinemann, J. A. Models of phage growth and their applicability to phage
793 therapy. *J. Theor. Biol.* **227**, 1–11 (2004).

794 18. Schrag, S. J. & Mittler, J. E. Host-Parasite Coexistence: The Role of Spatial Refuges in Stabilizing
795 Bacteria-Phage Interactions. *Am. Nat.* **148**, 348–377 (1996).

796 19. Santos, S. B., Carvalho, C., Azeredo, J. & Ferreira, E. C. Population Dynamics of a Salmonella Lytic
797 Phage and Its Host: Implications of the Host Bacterial Growth Rate in Modelling. *PLOS ONE* **9**,
798 e102507 (2014).

799 20. Kokjohn, T. A. & Sayler, G. S. Y. Attachment and replication of Pseudomonas aeruginosa
800 bacteriophages under conditions simulating aquatic environments. *Microbiology* **137**, 661–666
801 (1991).

802 21. Hadas, H., Einav, M., Fishov, I. & Zaritsky, A. Bacteriophage T4 Development Depends on the
803 Physiology of its Host Escherichia Coli. *Microbiology* **143**, 179–185 (1997).

804 22. Middelboe, M. Bacterial Growth Rate and Marine Virus–Host Dynamics. *Microb. Ecol.* **40**, 114–
805 124 (2000).

806 23. Nabergoj, D., Modic, P. & Podgornik, A. Effect of bacterial growth rate on bacteriophage
807 population growth rate. *MicrobiologyOpen* **7**, e00558 (2018).

808 24. Buckling, A. & Rainey, P. B. . Antagonistic coevolution between a bacterium and a
809 bacteriophage. *Proc. R. Soc. Lond. B Biol. Sci.* **269**, 931–936 (2002).

810 25. Volkova, V. V., Lu, Z., Besser, T. & Gröhn, Y. T. Modeling the Infection Dynamics of
811 Bacteriophages in Enteric Escherichia coli: Estimating the Contribution of Transduction to
812 Antimicrobial Gene Spread. *Appl. Environ. Microbiol.* **80**, 4350–4362 (2014).

813 26. Arya, S. *et al.* A generalised model for generalised transduction: the importance of co-evolution
814 and stochasticity in phage mediated antimicrobial resistance transfer. *FEMS Microbiol. Ecol.* **96**,
815 (2020).

816 27. Fillol-Salom, A. *et al.* Bacteriophages benefit from generalized transduction. *PLOS Pathog.* **15**,

817 e1007888 (2019).

818 28. Cassini, A. *et al.* Attributable deaths and disability-adjusted life-years caused by infections with
819 antibiotic-resistant bacteria in the EU and the European Economic Area in 2015: a population-
820 level modelling analysis. *Lancet Infect. Dis.* **19**, 56–66 (2019).

821 29. Lindsay, J. A. Staphylococcus aureus genomics and the impact of horizontal gene transfer. *Int. J.*
822 *Med. Microbiol.* **304**, 103–109 (2014).

823 30. Kifelew, L. G. *et al.* Efficacy of phage cocktail AB-SA01 therapy in diabetic mouse wound
824 infections caused by multidrug-resistant Staphylococcus aureus. *BMC Microbiol.* **20**, 204 (2020).

825 31. Petrovic Fabijan, A. *et al.* Safety of bacteriophage therapy in severe Staphylococcus aureus
826 infection. *Nat. Microbiol.* **5**, 465–472 (2020).

827 32. Abedon, S. T. & Katsaounis, T. I. Basic Phage Mathematics. in *Bacteriophages: Methods and*
828 *Protocols, Volume 3* (eds. Clokie, M. R. J., Kropinski, A. M. & Lavigne, R.) 3–30 (Springer, 2018).
829 doi:10.1007/978-1-4939-7343-9_1.

830 33. Christie, G. E. *et al.* The complete genomes of Staphylococcus aureus bacteriophages 80 and
831 80α—Implications for the specificity of SaPI mobilization. *Virology* **407**, 381–390 (2010).

832 34. Kasman, L. M. *et al.* Overcoming the Phage Replication Threshold: a Mathematical Model with
833 Implications for Phage Therapy. *J. Virol.* **76**, 5557–5564 (2002).

834 35. Eriksen, R. S., Mitarai, N. & Sneppen, K. Sustainability of spatially distributed bacteria-phage
835 systems. *Sci. Rep.* **10**, 3154 (2020).

836 36. Spiegelhalter, D. J., Best, N. G., Carlin, B. P. & Linde, A. V. D. Bayesian measures of model
837 complexity and fit. *J. R. Stat. Soc. Ser. B Stat. Methodol.* **64**, 583–639 (2002).

838 37. Sjöström, J.-E., Lindberg, M. & Philipson, L. Transfection of Staphylococcus aureus with
839 Bacteriophage Deoxyribonucleic Acid. *J. Bacteriol.* **109**, 285–291 (1972).

840 38. Berryhill, B. A., Huseby, D. L., McCall, I. C., Hughes, D. & Levin, B. R. Evaluating the potential
841 efficacy and limitations of a phage for joint antibiotic and phage therapy of Staphylococcus
842 aureus infections. *Proc. Natl. Acad. Sci.* **118**, (2021).

843 39. Gefen, O., Fridman, O., Ronin, I. & Balaban, N. Q. Direct observation of single stationary-phase
844 bacteria reveals a surprisingly long period of constant protein production activity. *Proc. Natl.*
845 *Acad. Sci.* **111**, 556–561 (2014).
846 40. Heijer, C. D. den *et al.* Prevalence and resistance of commensal Staphylococcus aureus, including
847 meticillin-resistant S aureus, in nine European countries: a cross-sectional study. *Lancet Infect.*
848 *Dis.* **13**, 409–415 (2013).
849 41. Stanczak-Mrozek, K. I. *et al.* Within-host diversity of MRSA antimicrobial resistances. *J.*
850 *Antimicrob. Chemother.* **70**, 2191–2198 (2015).
851 42. Suttle, C. A. & Chen, F. Mechanisms and Rates of Decay of Marine Viruses in Seawater. *Appl.*
852 *Environ. Microbiol.* **58**, 3721–3729 (1992).
853 43. Peterson, B. W., Sharma, P. K., van der Mei, H. C. & Busscher, H. J. Bacterial Cell Surface Damage
854 Due to Centrifugal Compaction. *Appl. Environ. Microbiol.* **78**, 120–125 (2012).
855 44. Chatterjee, A. N. Use of Bacteriophage-resistant Mutants to Study the Nature of the
856 Bacteriophage Receptor Site of Staphylococcus aureus. *J. Bacteriol*. **98**, 519–527 (1969).
857 45. Park, J. T., Shaw, D. R. D., Chatterjee, A. N., Mirelman, D. & Wu, T. Mutants of Staphylococci with
858 Altered Cell Walls. *Ann. N. Y. Acad*. Sci. **236**, 54–62 (1974).
859 46. Winstel, V., Xia, G. & Peschel, A. Pathways and roles of wall teichoic acid glycosylation in
860 Staphylococcus aureus. *Int. J. Med. Microbiol*. **304**, 215–221 (2014).
861 47. Xia, G., Kohler, T. & Peschel, A. The wall teichoic acid and lipoteichoic acid polymers of
862 Staphylococcus aureus. *Int. J. Med. Microbiol*. **300**, 148–154 (2010).48. Mašlaňová, I.,
863 Stříbná, S., Doškař, J. & Pantůček, R. Efficient plasmid transduction to Staphylococcus aureus
864 strains insensitive to the lytic action of transducing phage. *FEMS Microbiol. Lett.* **363**, (2016).
865 49. Jiang, S. C. & Paul, J. H. Gene Transfer by Transduction in the Marine Environment. *Appl.*
866 *Environ. Microbiol.* **64**, 2780–2787 (1998).
867 50. Fišarová, L. *et al.* Staphylococcus epidermidis Phages Transduce Antimicrobial Resistance
868 Plasmids and Mobilize Chromosomal Islands. *mSphere* **6**, (2021).

869 51. R Core Team. *R: A Language and Environment for Statistical Computing*. (R Foundation for
870 Statistical Computing, 2020).
871 52. Fey, P. D. *et al.* A Genetic Resource for Rapid and Comprehensive Phenotype Screening of
872 Nonessential Staphylococcus aureus Genes. *mBio* **4**, (2013).
873 53. Khan, S. A. & Novick, R. P. Complete nucleotide sequence of pT181, a tetracycline-resistance
874 plasmid from Staphylococcus aureus. *Plasmid* **10**, 251–259 (1983).
875 54. Veiga, H. & Pinho, M. G. Inactivation of the SauI Type I Restriction-Modification System Is Not
876 Sufficient To Generate Staphylococcus aureus Strains Capable of Efficiently Accepting Foreign
877 DNA. *Appl. Environ. Microbiol.* **75**, 3034–3038 (2009).
878 55. Adams, M. H. *Bacteriophages.* (Interscience Publishers, 1959).
879 56. Gelman, A. & Rubin, D. B. Inference from Iterative Simulation Using Multiple Sequences. *Stat.*
880 *Sci.* **7**, 457–472 (1992).